Journal of Fluids and Structures 27 (2011) 734–742

Contents lists available at ScienceDirect

Journal of Fluids and Structures

journal homepage: www.elsevier.com/locate/jfs

Wake stability features behind a square cylinder: Focus on small incidence angles

Gregory J. Sheard *

Department of Mechanical and Aerospace Engineering, Monash University, VIC 3800, Australia

ARTICLE INFO

Article history:
Received 20 October 2010
Received in revised form
1 February 2011
Accepted 18 February 2011
Available online 10 March 2011

Keywords:
Square cylinder
Three-dimensional transition
Bluff body
Floquet stability analysis
Quasi-periodic
Subharmonic

ABSTRACT

The stability of the flow behind a cylinder with a square cross-section is investigated with a focus on small incidence angles $0^\circ \le \alpha \le 12^\circ$. The first-occurring Mode A instability is found to be completely suppressed as the incidence angle is increased through $\alpha \approx 10.5^\circ$. The critical Reynolds number curve for the quasi-periodic mode is found to smoothly join the transition curve for the subharmonic mode. The switch from quasi-periodic to subharmonic properties occurs as α is increased from 2° to 3°, with no appreciable change in the structure of the leading eigenmode. Changes in the gradient of the critical Reynolds number curve with α, the gradient of the instability growth rate with Reynolds number, and the dominant spanwise wavelength demonstrate that the switch from quasi-periodic to subharmonic eigenvalues brings about subtle changes in the stability of the flow. The Reynolds number–incidence angle regimes for linear stability have been comprehensively mapped.

1. Introduction

The flow around bluff bodies continues to engender a significant amount of engineering research interest due to the myriad practical situations where obstacles are exposed to airflows or liquid flows. Cylinders of various cross-sections are of particular interest as they serve as a model for structures such as bridge spans and pylons, high-rise buildings, and offshore structures such as oil platforms and risers.

It is well known that the flow past a cylinder is a function of the Reynolds number, which relates inertial and viscous effects in a flow. At low Reynolds numbers the flows are steady and laminar, and at progressively higher Reynolds numbers the flow becomes more complicated, giving way firstly to time-dependent flow, and subsequently to three-dimensional instability before becoming turbulent. An understanding of three-dimensional transition in the flow past cylinders is important as it brings about abrupt changes in the frequency of vortex shedding, as well as lift and drag characteristics, which can have implications for the loading and fatigue of structures.

A tool which has been particularly successful for the analysis of three-dimensional transition in flows is linear stability analysis, which yields growth rates (σ) for small-amplitude three-dimensional instability modes of a selected spanwise wavelength (λ) growing on a two-dimensional base flow. Barkley and Henderson (1996) employed a Floquet-type linear stability analysis on the wake of a circular cylinder, and accurately determined the critical Reynolds number, spanwise wavelength, and spatio-temporal structure of the first-occurring three-dimensional instability. Named Mode A, this instability had been observed experimentally by Williamson (1988, 1996), and is found to emerge at a Reynolds number

* Tel.: +61 399051182.
E-mail address: Greg.Sheard@monash.edu

0889-9746/$ - see front matter © 2011 Elsevier Ltd. All rights reserved.
doi:10.1016/j.jfluidstructs.2011.02.005

(based on cylinder diameter and freestream velocity) of $Re \approx 180-190$. Mode A is characterized by a spanwise wavelength of approximately four times the cylinder diameter. With an increase in Reynolds number to $Re \approx 230-260$, Mode A gives way to a second three-dimensional mode, Mode B, which is characterized by a shorter spanwise wavelength of approximately 1 cylinder diameter. This second instability mode was also detected by the stability analysis of Barkley and Henderson (1996).

Modes A and B have since been found to be common to the wakes of other cylindrical bodies, such as slender rings with axis aligned with the free-stream (Sheard et al., 2003, 2004b), staggered tandem circular cylinders (Carmo et al., 2008), and square cylinders (Robichaux et al., 1999; Blackburn and Lopez, 2003). Despite differences between these geometries, Mode A typically occurs at a lower Reynolds number than Mode B, with a proportionally longer spanwise wavelength. Several studies have also detected a third instability mode in these systems. Behind circular cylinders (Blackburn et al., 2005) and square cylinders aligned at zero incidence to the oncoming flow (Blackburn and Lopez, 2003), a quasi-periodic mode is predicted, and behind rings (Sheard et al., 2005a,b) and inclined square cylinders (Sheard et al., 2009; Yoon et al., 2010, a subharmonic mode is predicted. Quasi-periodic modes are distinguished from subharmonic modes by the eigenvalues of the evolution operator of the linearized Navier–Stokes equations used to determine the stability of the flow. Quasi-periodic modes have a complex–conjugate pair of eigenvalues, whereas subharmonic modes have an eigenvalue on the negative real axis. These eigenvalues act as an amplification factor for the instability mode. Therefore a quasi-periodic mode has the physical effect of introducing a new frequency into the flow through the three-dimensional perturbation, whereas a subharmonic mode invokes an alternation in sign of the perturbation from one period to the next, resulting in a period-doubling of the flow once the instability develops. It has been shown analytically by Marques et al. (2004) that quasi-periodic modes are permitted in flows exhibiting a half-period reflective symmetry about the wake centreline (such as a square cylinder at zero incidence and a circular cylinder), whereas these systems do not permit a subharmonic mode. In contrast, subharmonic modes are permitted in systems which break this symmetry (such as slender rings or inclined square cylinders).

The system under investigation in this paper is that of a cylinder whose span is perpendicular to a uniform flow of speed U, with a square cross-section inclined at an angle α to the free-stream flow. For reference, this system is depicted in Fig. 1. The square cross-section has side length d, and the characteristic length is taken to be the projected height of the cylinder facing the oncoming flow, h. This gives a Reynolds number

$$Re = \frac{Uh}{\nu},$$

where ν is the kinematic viscosity of the fluid. The control parameters for the system are Re and α.

Laboratory investigations have been performed to investigate square cylinders at both a zero incidence (Luo et al., 2007) and at inclination (Tong et al., 2008). These studies employed dye visualization and hot-wire measurements to elucidate transitions in the flow, and proposed the first map of two- and three-dimensional regimes in the Reynolds number–incidence angle parameter space for inclined square cylinders. A linear stability analysis (Sheard et al., 2009), supported by direct numerical simulation, determined that the first-occurring three-dimensional transition behind inclined square cylinders was one of two instability modes: Mode A at incidence angles near 0° and 45°, and the subharmonic mode at intermediate angles. The subharmonic mode was most unstable at angles in the vicinity of 25°, and the transition Reynolds number increased substantially at incidence angles towards both 0° and 45°. At a zero incidence angle, Blackburn and Lopez (2003), Sheard et al. (2009) identified a quasi-periodic mode, which was predicted to become unstable well above the critical Reynolds numbers for Modes A and B. However, analysis was conducted at 7.5° increments in incidence angle, and no evidence of an unstable quasi-periodic mode was detected at or above 7.5°. This raised a question as to whether the subharmonic mode would immediately replace the quasi-periodic mode the instant that the wake symmetry was broken at non-zero incidence angles, or whether the quasi-periodic mode would persist to small non-zero angles.

Blackburn and Sheard (2010) sought to address this question by investigating the effect on the quasi-periodic mode of smoothly breaking reflective wake centreline symmetry. This was achieved using the strategies of inclining a square cylinder incrementally from zero to non-zero incidence angles, and by increasing the curvature of a slender ring from near zero. In both cases, it was found that the quasi-periodic mode persisted while the symmetry-breaking was small but finite, and when the asymmetry was further increased the complex–conjugate pair of eigenvalues smoothly migrated towards the negative real axis and split into a pair of subharmonic eigenvalues. In the context of flows around families of cylinder-like bodies, this study

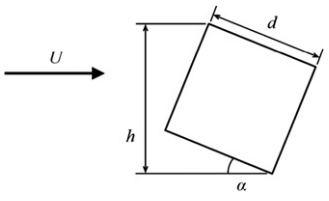

Fig. 1. A schematic representation of the inclined square-cylinder system, showing inclination angle α, characteristic length scale h, and free-stream velocity U.

demonstrated that the quasi-periodic and subharmonic mode branches are intrinsically linked: with changing wake symmetry, the quasi-periodic mode *changes into* the subharmonic mode, rather than being *replaced* by it through the emergence of a distinct eigenvalue.

A more recent numerical study (Yoon et al., 2010) calculated the stability of an inclined square cylinder flow at a number of additional incidence angles, refining the Reynolds number–incidence angle regime map. Two notable features arose from their results: firstly, in keeping with the results of Blackburn and Sheard (2010), the quasi-periodic mode branch was found to extend to non-zero incidence angles (they detected the quasi-periodic mode up to approximately 2°, but included no data on the quasi-periodic/subharmonic branch up to $\alpha = 10.2^\circ$), and secondly, while interpolation suggested in Sheard et al. (2009) that the crossover from Mode A to the subharmonic mode occurred at approximately 12°, Yoon et al. (2010) detected the subharmonic mode and not Mode A at a lower angle of 10.2°. Thus Sheard et al. (2009) over-estimated the threshold incidence angle for the crossover from Mode A to the subharmonic mode. Instead of occurring at approximately 12°, and accounting for the data in Yoon et al. (2010), the crossover could potentially occur anywhere down to 7.5°. Furthermore, why is Mode A not detected at all at $\alpha = 10.2^\circ$? The present study is motivated to resolve these questions by way of the most detailed linear stability analysis yet conducted on the inclined square cylinder system.

2. Numerical treatment

This investigation requires the computation of two-dimensional flows serving as the basis for linear stability analysis. A two-dimensional solver using a nodal spectral element method for spatial discretization and a third-order time integration scheme based on backwards differentiation is used (Sheard et al., 2007; Neild et al., 2010; Hussam et al., 2011; Sheard and King, 2011) to solve the time-dependent incompressible Navier–Stokes equations. Linear stability analysis is performed by evolving a three-dimensional perturbation on the two-dimensional base flow using the linearized Navier–Stokes equations. The ARPACK eigenvalue solver (Lehoucq et al., 1998) is employed to determine the leading eigenmodes of the stability problem, where eigenvalues correspond to Floquet multipliers (μ), and eigenvectors yield the mode shape of the perturbation field. For details see Sheard et al. (2009) and Blackburn and Sheard (2010). Floquet multipliers represent amplification factors, and relate to the exponential growth rates (σ) of modes through $\sigma = \log|\mu|/T$, where T is the temporal period of the base flow. A Floquet multiplier with $|\mu| > 1$ corresponds to a positive growth rate ($\sigma > 0$) and an unstable mode.

The meshes used in this study were adapted from those employed for the square-cylinder calculations in Blackburn and Sheard (2010). The domain size and element distribution was kept consistent across all incidence angles, and a rotational distortion was applied to the region of the mesh in the vicinity of the cylinder cross-section to facilitate the range of incidence angles being modelled. The meshes comprised 644 elements, each of polynomial degree 9. A rectangular domain surrounded the square cylinder, which in these computations scaled with h. The distances from the cylinder to the upstream, transverse, and downstream boundaries were $20h$, $20h$, and $35h$, respectively. On all boundaries except the downstream boundary a high-order Neumann pressure gradient boundary condition was constructed (as per Karniadakis et al., 1991) to preserve the third-order time accuracy of the computations. On the downstream boundary a constant reference pressure was imposed, combined with a zero velocity gradient normal to the boundary. A uniform horizontal velocity was imposed at the upstream boundary, stress-free conditions were imposed on the transverse boundaries to minimize blockage effects, and a no-slip condition was imposed on velocity at the surface of the cylinder.

As the goal of this investigation is to develop a detailed picture of the transition regimes at small incidence angles, meshes were constructed at one-degree incidence-angle increments over $0^\circ \le \alpha \le 12^\circ$, with the exception that a mesh for $\alpha = 10.2^\circ$ was constructed instead of 10° to better facilitate comparison with Yoon et al. (2010). Approximate critical Reynolds numbers for transition could be inferred from Tong et al. (2008), Sheard et al. (2009), and Yoon et al. (2010), and thus the stability analysis could be targeted at narrow ranges of Reynolds numbers and spanwise wavelengths in close proximity to the dominant modes, minimizing the intervals between data points and enhancing the precision of the predictions. Polynomial interpolation was used to determine the wavenumber m (which relates to the spanwise wavelength through $\lambda/h = 2\pi/m$) giving the highest growth rate for an instability mode at a given Reynolds number. Subsequently, interpolation was performed across Reynolds numbers to find the critical Reynolds number at which the mode peak first becomes neutrally stable (i.e. zero growth rate), and the wavenumber at which this occurs. Typically, 15–20 Floquet multipliers were computed to obtain each critical Reynolds number in the results to follow.

3. Results

3.1. The Mode A branch

The first mode to be considered is the Mode A instability. Here an explanation for the absence of an unstable Mode A instability at $\alpha = 10.2^\circ$ from the calculations of Yoon et al. (2010) is sought. Fig. 2 shows the key Reynolds number curves for the Mode A instability branch at small angles. At $\alpha = 0^\circ$, the present stability calculations for the onset of the Mode A instability are in agreement with Sheard et al. (2009), predicting $Re_{\mathrm{crit}} = 164$ at a wavenumber $m = 1.24$. With an increase in α, the critical Reynolds number for the onset of the Mode A instability also increases. Unusually, for a given α, the predicted

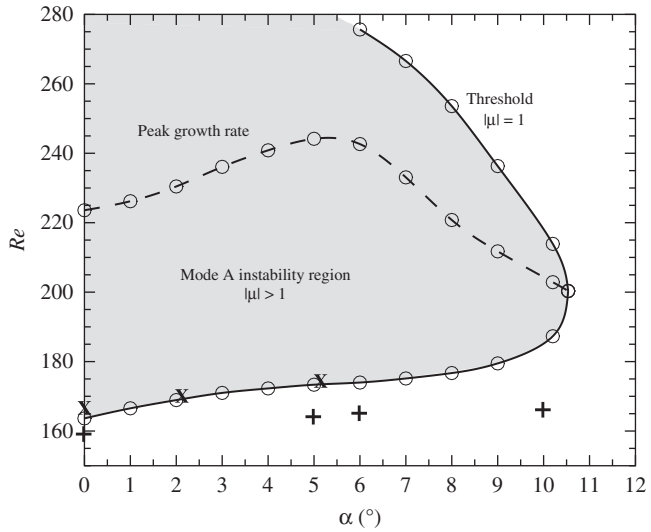

Fig. 2. Critical Reynolds numbers for the Mode A instability plotted against incidence angle. The unstable region of the parameter space is shaded, and a dashed line marks the point at which the maximum growth rate was found in the Mode A waveband for each incidence angle. Critical Reynolds numbers from the linear stability analysis of Yoon et al. (2010) (×) and the experiments of Tong et al. (2008) (+) are included, and show a good agreement with the present data.

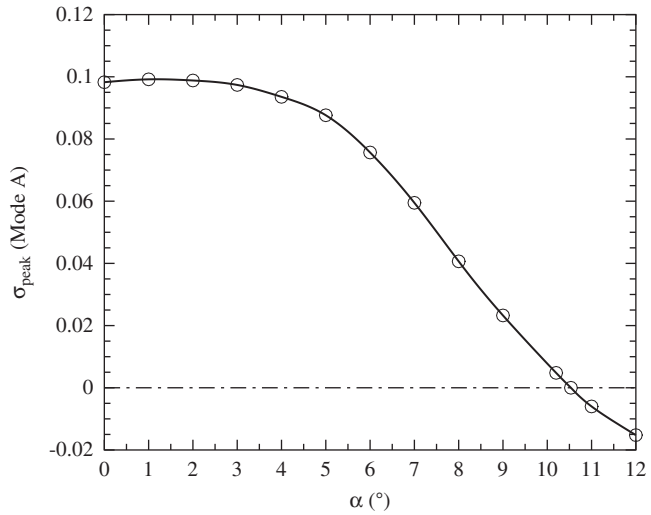

Fig. 3. Peak growth rate for the Mode A instability plotted against incidence angle. The horizontal dash-dotted line marks the neutral stability threshold ($\sigma = 0$).

growth rate of the Mode A instability did not increase monotonically for all Reynolds numbers in the range covered in this analysis. Instead, the growth rate reached a maximum value, before subsequently decreasing again at higher Reynolds numbers. The peak Reynolds number for Mode A is predicted to occur at Re=224 at $\alpha = 0^\circ$; it increased to Re=244 at $\alpha \approx 5^\circ$; and at higher α the peak occurs at lower Reynolds numbers. The growth rate drops sufficiently beyond the peak Reynolds numbers that beyond $\alpha \approx 6^\circ$, Reynolds numbers were found where the Mode A waveband only achieved negative growth rates. Thus the flow was only unstable to Mode A over a finite range of Reynolds numbers. The Reynolds number window where Mode A was unstable progressively shrinks at higher incidence angle, and these computations predict that when α reaches 10.5°, the Mode A waveband is not unstable for any Reynolds numbers in the range considered in this study. At $\alpha = 10.5^\circ$, the critical Reynolds number at which Mode A grazes the neutral stability threshold ($\sigma = 0$) is Re=200.

Thus it may be concluded that the flow becomes less sensitive to the Mode A instability as the incidence angle is increased from 0°. A confirmation of this observation is shown in Fig. 3, which plots the peak growth rate of the Mode A instability against incidence angle. This plot verifies that beyond $\alpha = 10.5^\circ$, the Mode A instability is suppressed. This result permits an interesting interpretation of dye visualization results presented in Tong et al. (2008). In that study, dye

visualization identified three-dimensional wake structures resembling Mode A behind a square cylinder at $\alpha = 0^\circ$ and 10°. However, these structures were significantly stronger at 0° than at 10°. It is possible that the substantially smaller growth rates at 10°, or the narrower range of Reynolds numbers yielding positive growth rates, lead to a smaller amplitude of the saturated structure arising from these instability modes, thus producing the weaker Mode A structures at 10° relative to 0°. For further reading on non-linear evolution and saturation of three-dimensional wake flows, the reader should consult Sheard et al. (2004a,b) and Carmo et al. (2008).

The prediction of positive growth rates for the Mode A instability in these computations at $\alpha = 10.2^\circ$ (and indeed up to $\alpha = 10.5^\circ$) is in contrast to Yoon et al. (2010), where Mode A was not detected at $\alpha = 10.2^\circ$. Given the close (but not exact) agreement between their critical Reynolds number curves and those of Sheard et al. (2009), the differences between the two sets of computations may be attributed to the different domain sizes and numerical techniques employed in the two studies. Thus the suppression of Mode A most likely occurred at an incidence angle just below $\alpha = 10.2^\circ$ in their model, explaining their detection of only the subharmonic (Mode C) instability at that incidence angle.

3.2. Subharmonic and quasi-periodic modes

The critical Reynolds number curve for the quasi-periodic/subharmonic mode branch is shown in Fig. 4. Blackburn and Sheard (2010) showed that the transition from quasi-periodic to subharmonic eigenvalues occurred at an incidence angle of $\alpha = 5.9^\circ$ for a cylinder with a square cross-section. That study conducted the stability analysis at a constant Reynolds number (based on the cylinder side length) of Re_d=225. At $\alpha = 5.9^\circ$, this corresponds to a Reynolds number here of Re=247. At that Reynolds number the Floquet multiplier resided inside the unit circle ($|\mu| < 1$), which corresponds to a decaying mode and a stable flow. In this study the nature of the eigenvalues of the instability modes has been ascertained precisely at the transition Reynolds number as well as at the peak wavenumber for all incidence angles. It is found at the critical Reynolds number that the crossover between the quasi-periodic mode and the subharmonic mode takes place somewhere between $\alpha = 2^\circ$ and 3°. This supports Yoon et al. (2010), where a quasi-periodic mode was detected at $\alpha \approx 2^\circ$.

At $\alpha = 0^\circ$, the mode is found to be quasi-periodic, with a critical Reynolds number of Re_c=214. This value is again consistent with earlier studies (Sheard et al., 2009). The critical Reynolds number increases with incidence angle to a maximum of $Re_c \approx 260$ at $\alpha \approx 6^\circ$, before subsequently decreasing with further increases in α. The trend of the critical Reynolds number rising over $0^\circ \leq \alpha \lesssim 6^\circ$ and falling beyond $\alpha \approx 6^\circ$ closely mirrors the trend in the maximum growth rate of the Mode A instability.

It is notable that while the critical Reynolds number curve continues to increase through the transition from quasi-periodic to subharmonic eigenvalues, there is a perceptible shift in gradient through the transition. The implications of this observation are explored further in the following section, where the spanwise wavelengths of the instabilities are considered.

The dominant Floquet multipliers at the critical Reynolds number are plotted on the complex plane in Fig. 5 which verifies that breaking symmetry by increasing α from 0° causes the phase angle of the complex eigenvalue to shift towards the negative real axis, where the mode becomes subharmonic. As in Blackburn and Sheard (2010), the initial stages of symmetry breaking result in a modest shift in the eigenvalue, whereas the rate at which the eigenvalue approaches the

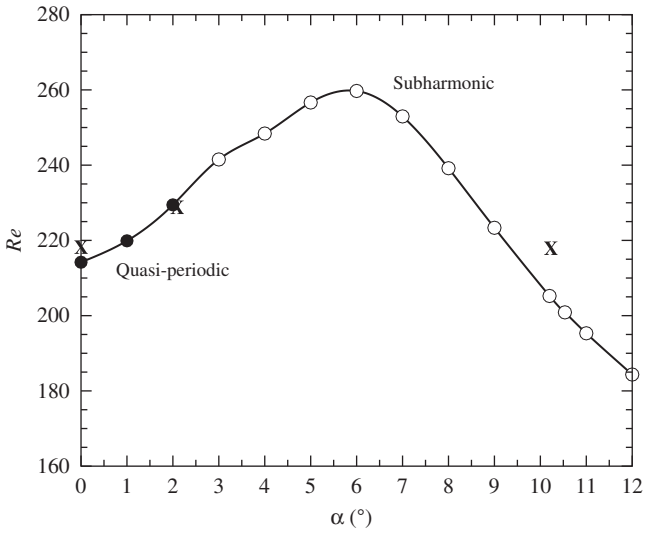

Fig. 4. Critical Reynolds numbers for the quasi-periodic and subharmonic modes plotted against incidence angle. Black and white symbols (○) denote modes with quasi-periodic and subharmonic eigenvalues, respectively, and a spline is fitted to the present data for guidance. For comparison, the predicted critical Reynolds numbers for this mode branch from the linear stability analysis of Yoon et al. (2010) (×) are also included.

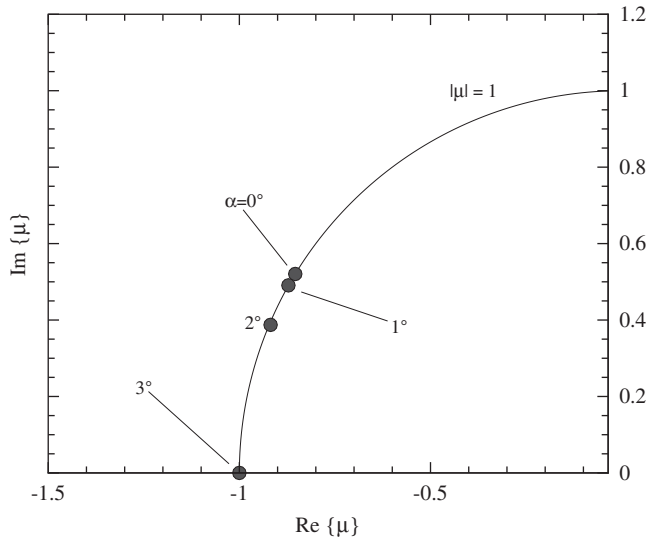

Fig. 5. Floquet multipliers at the dominant wavenumber and critical Reynolds number for the quasi-periodic/subharmonic mode branch plotted on the complex plane. At $\alpha = 0-2^{\circ}$, the eigenvalues are quasi-periodic, as they contain an imaginary component. For $\alpha \gtrsim 3^{\circ}$, the dominant eigenvalue is subharmonic. The eigenvalues all exhibit $|\mu| = 1$, demonstrating neutral stability at the critical Reynolds number.

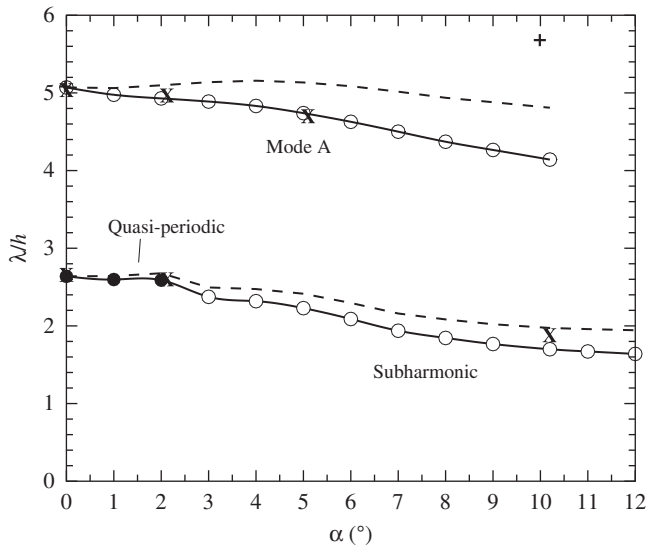

Fig. 6. Spanwise wavelengths plotted against incidence angle for Mode A and the quasi-periodic and subharmonic modes. Black and white symbols differentiate quasi-periodic and subharmonic modes, respectively, and the Mode A wavelengths are denoted by open symbols. Dashed lines show the spanwise wavelengths scaled by the side length of the square cylinder cross-section (d), rather than h. Data from Yoon et al. (2010) (×) and the experiments of Tong et al. (2008) (+) are included for comparison.

negative real axis increases substantially as α approaches the critical incidence angle for the quasi-periodic/subharmonic changeover.

3.3. Spanwise wavelengths of the instability mode branches

Fig. 6 shows the variation in the dominant spanwise wavelengths of both the Mode A instability and the quasi-periodic/subharmonic modes. Two normalizations are used for the spanwise wavelengths: h and d. When normalized by d, the spanwise wavelength for the Mode A instability remains almost consistently at $\lambda/d \approx 5$. This demonstrates that the Mode A instability scales with d rather than the projected height h. This scaling is not observed for the quasi-periodic/subharmonic mode as the incidence angle is varied. Instead, the spanwise wavelength decreases by approximately 25% and 40% from

$\alpha = 0^\circ$ to 12° when normalized by d and h, respectively. The current results agree well with the linear stability analysis of Yoon et al. (2010). The spanwise wavelength data from Tong et al. (2008), which was obtained using an autocorrelation method, are qualitatively consistent with the present predictions. It is noted that laboratory conditions such as finite

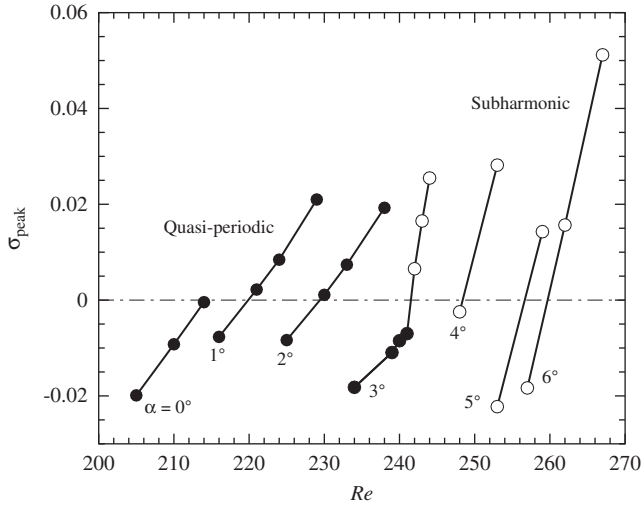

Fig. 7. Dominant growth rate (σ) plotted against Reynolds number in the vicinity of neutral stability for the quasi-periodic/subharmonic waveband. Data are shown for incidence angles $0^\circ \le \alpha \le 6^\circ$ as labelled.

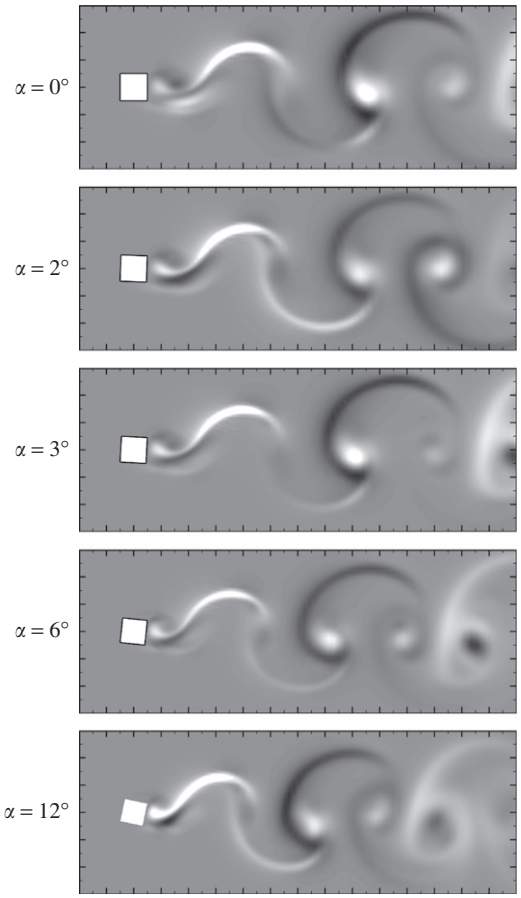

Fig. 8. Contour plots of the horizontal component of velocity in the perturbation field of the dominant mode in the quasi-periodic/subharmonic waveband at the neutral stability threshold (the curve in Fig. 4) at several incidence angles. Light and dark shadings correspond to positive and negative velocities, respectively.

cylinder span, end effects, and background noise can restrict the available spanwise wavelengths adopted by the instability mode; this may explain the discrepancy between the predicted and measured wavelengths at $\alpha \approx 10^{\circ}$.

The shift from quasi-periodic to subharmonic eigenvalues can be seen to cause a noticeable decrease in the peak spanwise wavelength of the mode. This suggests that while there is a smooth shift in the eigenvalue on the complex plane through this change, the stability of the flow has undergone a significant change. A complementary view of this behaviour can be found in Fig. 7, which shows the Reynolds-number dependence of the dominant growth rate of the quasi-periodic/subharmonic waveband at difference incidence angles. It is apparent that in the quasi-periodic regime, the gradient $\mathrm{d}\sigma/\mathrm{d}Re \approx 0.002$, which is noticeably shallower than in the subharmonic regime, where the gradient increases more than three-fold to $\mathrm{d}\sigma/\mathrm{d}Re \approx 0.006-0.010$. This suggests that the driving mechanism for the subharmonic instability is distinct from that of the quasi-periodic instability, despite the close physical relationship between the two modes. Highlighting the close relationship between the quasi-periodic and subharmonic states, Fig. 8 shows the perturbation fields at several incidence angles along the neutral stability curve for this mode. The topology of the perturbation field flow structures are qualitatively consistent across these incidence angles, supporting the view that the quasi-periodic and subharmonic regimes are part of the one mode branch. No discernable change in structure is observed through the switch between these regimes.

4. The new regime map and concluding remarks

The computations performed in this study provide a clearer picture of the stability of the wake behind an inclined square cylinder than was available from earlier attempts to map these regimes (Sheard et al., 2009; Yoon et al., 2010). Fig. 9 shows the revised regime map arising from these simulations. This study has demonstrated that with increasing incidence angle from $\alpha = 0^{\circ}$, the flow is initially first unstable to the Mode A instability. This mode is progressively suppressed, so that by $\alpha = 10.5^{\circ}$ the flow is no longer unstable to Mode A. Thereafter the first-occurring instability is succeeded by the subharmonic Mode C instability. As the incidence angle approaches 45°, which corresponds to a recovery of reflective symmetry about the wake centreline, Sheard et al. (2009) showed that Mode C is replaced again by Mode A as the first-occurring instability mode. This is indicated in Fig. 9 at $\alpha \approx 26^{\circ}$.

This study has also shown for the first time the unbroken critical Reynolds number curve for the quasi-periodic/subharmonic mode branch. Although this mode is not the first-occurring instability for $\alpha < 10.5^{\circ}$, and therefore may not be detectable at these incidence angles in a physical setting because of the distortion of the flow by the prior Mode A instability, its completion is important from the perspective of understanding the relationship between quasi-periodic and subharmonic instability modes in wake flows. Following verification that eigenvalues smoothly change from quasi-periodic to subharmonic at a finite symmetry-breaking control parameter (Blackburn and Sheard, 2010), this study has shown that at the critical Reynolds number, the second-occurring three-dimensional instability is quasi-periodic at incidence angles $\alpha \lesssim 2^{\circ}$, and is subharmonic at larger incidence angles.

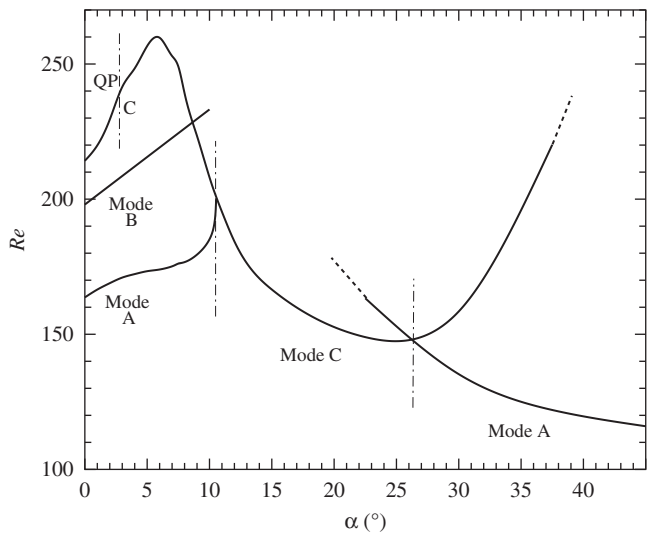

Fig. 9. The updated regime map for linear instability modes in the wakes behind inclined square cylinders, with critical Reynolds number curves plotted against incidence angle. The various modes are labelled, and dash-dotted lines are used to mark important incidence angles in the parameter space. The terms "QP" and "C" refer to the quasi-periodic and subharmonic (Mode C) parts of that transition curve.

Acknowledgements

This work was supported by a Monash University Faculty of Engineering Small Grant. Simulations were performed using the resources of the National Computational Infrastructure National Facility. NCI is supported by the Australian Commonwealth Government. The author's attendance at the IUTAM Symposium on Bluff Body Wakes and Vortex-Induced Vibrations (BBVIV-6, Capri, Italy, 22–25 June 2010), where this work was first presented, was supported in part by the Department of Mechanical and Aerospace Engineering, Monash University.

References

Barkley, D., Henderson, R.D., 1996. Three-dimensional Floquet stability analysis of the wake of a circular cylinder. Journal of Fluid Mechanics 322, 215–241.

Blackburn, H.M., Lopez, J.M., 2003. On three-dimensional quasi-periodic Floquet instabilities of two-dimensional bluff body wakes. Physics of Fluids 15, L57–L60.

Blackburn, H.M., Marques, F., Lopez, J.M., 2005. Symmetry breaking of two-dimensional time-periodic wakes. Journal of Fluid Mechanics 522, 395–411.

Blackburn, H.M., Sheard, G.J., 2010. On quasi-periodic and subharmonic Floquet wake instabilities. Physics of Fluids 22, 031701.

Carmo, B.S., Sherwin, S.J., Bearman, P.W., Willden, R.H.J., 2008. Wake transition in the flow around two circular cylinders in staggered arrangements. Journal of Fluid Mechanics 597, 1–29.

Hussam, W.K., Thompson, M.C., Sheard, G.J., 2011. Dynamics and heat transfer in a quasi-two-dimensional MHD flow past a circular cylinder in a duct at high Hartmann number. International Journal of Heat and Mass Transfer 54, 1091–1100.

Karniadakis, G.E., Israeli, M., Orszag, S.A., 1991. High-order splitting methods for the incompressible Navier–Stokes equations. Journal of Computational Physics 97, 414–443.

Lehoucq, R.B., Sorenson, D.C., Yang, C., 1998. ARPACK Users' Guide. SIAM, Philadelphia, PA.

Luo, S.C., Tong, X.H., Khoo, B.C., 2007. Transition phenomena in the wake of a square cylinder. Journal of Fluids and Structures 23, 227–248.

Marques, F., Lopez, J.M., Blackburn, H.M., 2004. Bifurcations in systems with Z_2 spatio-temporal and $O(2)$ spatial symmetry. Physica D 189, 247–276.

Neild, A., Ng, T.W., Sheard, G.J., Powers, M., Oberti, S., 2010. Swirl mixing at microfluidic junctions due to low frequency side channel fluidic perturbations. Sensors and Actuators B: Chemical 150, 811–818.

Robichaux, J., Balachandar, S., Vanka, S.P., 1999. Three-dimensional Floquet instability of the wake of a square cylinder. Physics of Fluids 11, 560–578.

Sheard, G.J., Fitzgerald, M.J., Ryan, K., 2009. Cylinders with square cross section: wake instabilities with incidence angle variation. Journal of Fluid Mechanics 630, 43–69.

Sheard, G.J., King, M.P., 2011. Horizontal convection: effect of aspect ratio on Rayleigh-number scaling and stability. Applied Mathematical Modelling 35, 1647–1655.

Sheard, G.J., Leweke, T., Thompson, M.C., Hourigan, K., 2007. Flow around an impulsively arrested circular cylinder. Physics of Fluids 19, 083601.

Sheard, G.J., Thompson, M.C., Hourigan, K., 2003. From spheres to circular cylinders: the stability and flow structures of bluff ring wakes. Journal of Fluid Mechanics 492, 147–180.

Sheard, G.J., Thompson, M.C., Hourigan, K., 2004a. Asymmetric structure and non-linear transition behaviour of the wakes of toroidal bodies. European Journal of Mechanics B/Fluids 23, 167–179.

Sheard, G.J., Thompson, M.C., Hourigan, K., 2004b. From spheres to circular cylinders: non-axisymmetric transitions in the flow past rings. Journal of Fluid Mechanics 506, 45–78.

Sheard, G.J., Thompson, M.C., Hourigan, K., 2005a. The subharmonic mechanism of the Mode C instability. Physics of Fluids 17, 111702.

Sheard, G.J., Thompson, M.C., Hourigan, K., Leweke, T., 2005b. The evolution of a subharmonic mode in a vortex street. Journal of Fluid Mechanics 534, 23–38.

Tong, X.H., Luo, S.C., Khoo, B.C., 2008. Transition phenomena in the wake of an inclined square cylinder. Journal of Fluids and Structures 24, 994–1005.

Williamson, C.H.K., 1988. The existence of two stages in the transition to three-dimensionality of a cylinder wake. Physics of Fluids 31, 3165–3168.

Williamson, C.H.K., 1996. Mode A secondary instability in wake transition. Physics of Fluids 8, 1680–1682.

Yoon, D.H., Yang, K.S., Choi, C.B., 2010. Flow past a square cylinder with an angle of incidence. Physics of Fluids 22, 043603.